

A Novel AC–DC Step-Up Converter For Energy Harvesting

S.VENKAT RAO¹, A.BALAJI²

¹Assistant Professor Department. Of Electrical & Electronics Engineering Sri Venkatesa Perumal College of Engineering & Technology

²PG Student Department. Of Electrical & Electronics Engineering Sri Venkatesa Perumal College of Engineering & Technology

Abstract:- The conventional two-stage power converters with bridge rectifiers are inefficient and may not be practical for the low-voltage microgenerators. This paper presents an efficient ac-to-dc power converter that avoids the bridge rectification and directly converts the low ac input voltage to the required high dc output voltage at a higher efficiency. The proposed converter consists of a boost converter in parallel with a buck-boost converter, which are operated in the positive half cycle and negative half cycle, respectively. Detailed analysis of the converter is carried out to obtain relations between the power, circuit parameters, and duty cycle of the converter. Based on the analysis, control schemes are proposed to operate the converter. Design guidelines are presented for selecting the converter component and control parameters. A self-starting circuit is proposed for independent operation of the converter. Detailed loss calculation of the converter is carried out. Simulation results are presented to validate the proposed converter topology and control schemes.

Index Terms:- AC–DC conversion, boost converter, energy harvesting, low power, low voltage, power converter control.

I. INTRODUCTION

SELF-POWERED devices harvest the ambient energies by microgenerators and can perform their operations without any continuous external power supply. Many types of micro-generators, used in the self-powered devices, are reported in the literature for harvesting different forms of ambient energies [1]–[8]. The inertial microgenerators, which harvest mechanical energy from the ambient vibrations, are currently the focus of many research groups [2]–[6], [8]–[13], [16]–[21]. The power level of the inertial microgenerators is normally very low, ranging from few microwatts to tens of milliwatts. Based on the energy conversion principle, the inertial microgenerators can be classified mainly into three types: electromagnetic, piezo-electric, and electrostatic [5]–[10], [12]–[16]. Among them, the electromagnetic microgenerators have the highest energy density [8], [9], [20]. In this research, the electromagnetic micro-generators are considered for further study.

The electromagnetic generators are typically spring-mass-damper-based resonance systems (see Fig. 1) in which the small amplitude ambient mechanical vibrations are amplified into larger amplitude translational movements and the mechanical

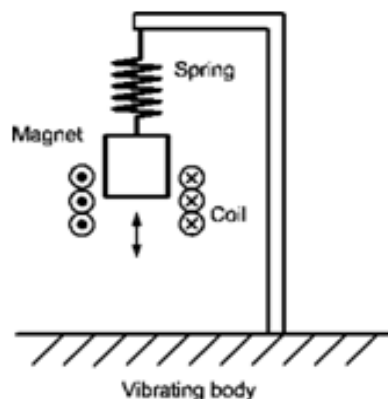


Fig. 1. Schematic diagram of a resonance inertial microgenerator.

energy of the motion is converted to electrical energy by electromagnetic coupling [9]. The output voltage of an electromagnetic microgenerator is ac type, but the electronic loads require dc voltage for their operation. Therefore, the ac voltage of the electromagnetic microgenerator output has to be processed by a suitable power

converter to produce the required dc voltage for the load.

One of the challenges with the electromagnetic micro-generators is that, due to the practical size limitations, the output voltage level of the generators is very low (few hundreds of millivolts), whereas the electronic loads require much higher dc voltage (3.3 V) [9]. The conventional power converters, re-ported for energy harvesting [2]–[7], [10], [11], [14]–[18], [20], [22], mostly consist of two stages: a diode bridge rectifier and a standard buck or boost dc-to-dc converter [see Fig. 2(a)]. However, there are major disadvantages in using the two-stage power converters to condition the outputs of the electromagnetic microgenerators. First, for very low-voltage electromagnetic microgenerators, rectification is not feasible by the use of conventional diodes. Second, if the diode bridge rectification is feasible, the forward voltage drops in the diodes will cause a large amount of losses and make the power conversion very inefficient.

To address the problems of the conventional two-stage con-verters, direct ac-to-dc converters are proposed [10], [13], [15]. In these converters, bridge rectification is avoided and the micro-generator power is processed only in a single-stage boost-type power converter [see Fig. 2(b)]. A dual-polarity boost converter topology for direct ac-to-dc power converter is

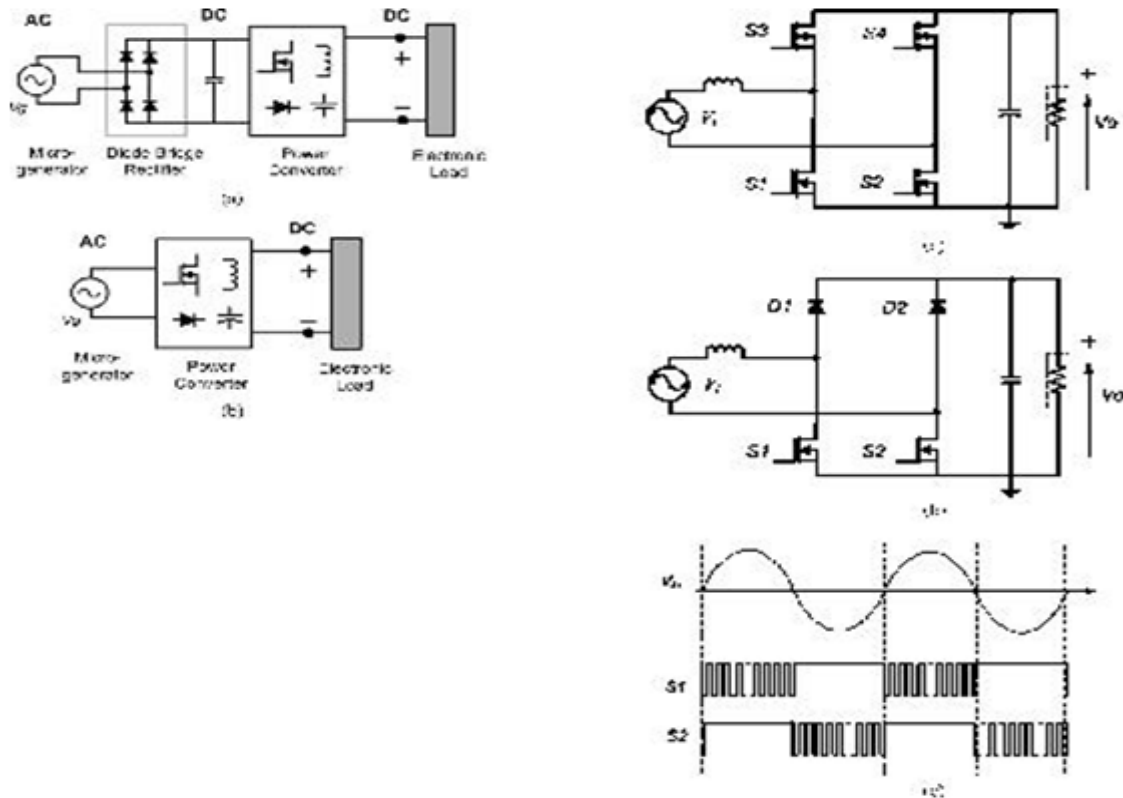


Fig. 2. Block diagrams. (a) Conventional two-stage power conversion con-sisting diode bridge rectifier. (b) Direct ac-to-dc power conversion.

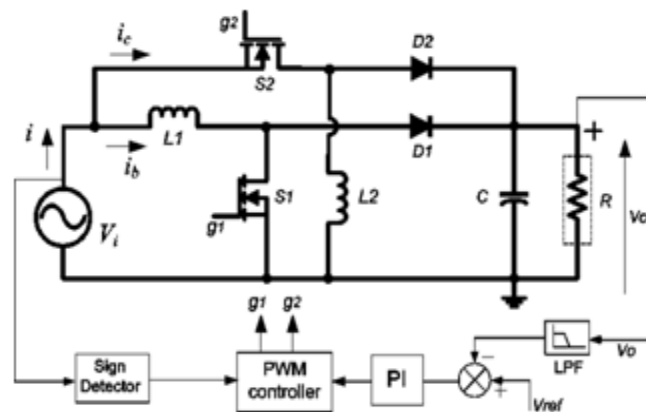


Fig. 3. Proposed direct ac-to-dc converter.

Fig. 4. (a) Standard 4-switch H-bridge ac–dc boost converter. (b) 2-switch H-bridge boost converter. (c) Input voltage and the gate drive pulsed to the lower switches (S_1 and S_2).

large voltage drops will occur in the capacitors during the half cycles when they are not charged by the converter. Extremely large capacitors will be required to achieve acceptable voltage ripple at the output dc bus. This is not practical due to the size limitations of the microgenerators.

A direct ac-to-dc converter is proposed in [21]. The proposed converter, as shown in Fig. 3, consists of a boost converter (inductor L_1 , switch S_1 , and diode, D_1) in parallel with a buck–boost converter (inductor L_2 , switch S_2 , and diode D_2). In this converter, the negative output to input voltage gain of a buck–boost converter is utilized to step-up the negative half input voltage of the microgenerator to a positive high-dc output voltage. The output dc bus is realized by using a single capacitor. The output capacitor is charged by the boost converter in the positive half cycle and by the buck–boost converter in the negative half cycle. Therefore, it resolves the problems present in a dual-polarity boost converter.

The standard 4-switch H-bridge converter or the 2-switch H-bridge converter, as shown in Fig. 4(a) and (b) respectively, can be used for the direct ac-to-dc boost conversion [23]. It can be noted that to achieve the boost operation, the lower switches

(S_1 and S_2) of these two converters should be able to conduct in both the directions. In this case, without increasing the number of devices, the bidirectional conduction capability of the two MOSFETs (S_1 and S_2) can be used to achieve the boost operation. The control gate pulses for these two switches are shown in Fig. 4(c). It can be seen that during the positive half cycle of the input voltage, S_2 is kept ON for the entire half cycle and the gate pulse to S_1 is controlled to achieve the boost operation. Likewise, in the negative half cycle, S_1 is kept ON for the entire half cycle and S_2 is controlled. To achieve the boost operation, these two topologies use single inductor compared to the two inductors used in the proposed converter in this study (see Fig. 3). However, there are several disadvantages in these two H-bridge converters. First, in these converters, there are two devices in the conduction path during charge or discharge of the boost inductor. In the proposed converter, only a single device conducts during the charge or discharge of the inductors. In the converter, proposed in this paper, any MOSFET is operated only for a half cycle of the input ac voltage, whereas, in the H-bridge-type converters, the MOSFETs, used for the boost operation (S_1 and S_2), are operated for the entire cycle of the input ac voltage. Therefore, the device conduction losses in the proposed converter are reduced by more than a factor of two. In energy harvesting applications, as the power level is very low, these losses are significant compared to the total output power. Second, as the MOSFETs are designed for forward conduction, in the reverse conduction mode they offer higher ON-state resistance. This further increases the conduction losses in the H-bridge topologies. Third, the input voltage polarity has to be sensed to control S_1 and S_2 , but in the H-bridge topologies, the input voltage source is floating with respect to the output voltage ground. Therefore, the implementation of the control circuit is difficult. This can be easily implemented in the proposed converter. Furthermore, it can be mentioned that although the proposed converter uses two inductors (L_1 and L_2), they do not operate in the same half cycle. Therefore, their total losses are almost equal to the losses of the single inductor used in the H-bridge converters.

In this paper, detailed analysis of the proposed converter is presented. Closed form relations are derived between the input power, the input frequency, the duty cycle, and various circuit parameters of the converter. Based on this analysis, appropriate control schemes are proposed to operate the converter. For high voltage step-up application, a simplified control strategy is presented that uses equal inductors for both converters. Design guidelines are presented to select the components of the converter. A converter is designed based on the analysis. In a practical energy-harvesting scenario, the controller and the MOSFET driver circuit of the converter are required to be self-starting and they should be powered by the energy harvesting system. In this paper, an auxiliary self-starting power circuit is proposed for powering the controller and the MOSFET drivers. The operations and the implementations of the control scheme and the self-starting circuits are presented in detail. Simulations are carried out for the verification of the design, the proposed control schemes, and the proposed self-starting circuit.

The rest of the paper is organized in the following manner: Section II presents detailed analysis of the converter and the proposed control schemes to control the converter. Section III presents the design guidelines for the selection of the converter parameters. Section IV presents the proposed self-starting circuit and the converter control circuit implementation. Simulations are presented in Section V. Finally the conclusion is presented.

II. DIRECT AC-TO-DC CONVERTER

The electromagnetic microgenerators typically consist of a moving permanent magnet, linking flux with a stationary coil (see Fig. 1). The variation of the flux linkage induces ac voltage in the coil. The typical output voltage of an electromagnetic microgenerator is sinusoidal. Hence, in this study, the microgenerator is modeled as a sinusoidal ac voltage source. Furthermore, electromagnetic microgenerators with low output

voltages (few hundreds of millivolts) are only considered in this study for energy harvesting.

The proposed direct ac-to-dc power conditioning circuit, as shown in Fig. 2, consists of one boost converter in parallel with one buck–boost converter. The output capacitor C of this converter is charged by the boost converter (comprising inductor L_1 , switch S_1 , and diode, D_1) and the buck–boost converter (comprising inductor L_2 , switch S_2 , and diode D_2) during the positive half cycles and the negative half cycles of the sinusoidal ac input voltage (v_i), respectively. n-channel MOSFETs are utilized to realize the switches S_1 and S_2 . It can be noted that the MOSFETs are subjected to reverse voltage by the ac output of the microgenerator. To block the reverse conduction, the forward voltage drop of the body diodes of the MOSFETs is chosen to be higher than the peak of the input ac voltage. Two schottky diodes (D_1 and D_2) with low forward voltage drop are used in the boost and the buck–boost converter circuits for low losses in the diodes. It can be mentioned that the diodes can be replaced by MOSFETs to further improve the efficiency of the converter.

The proposed converter is operated under discontinuous mode of operation (DCM). This reduces the switch turn ON and turn OFF losses. The DCM operation also reduces the diode reverse recovery losses of the boost and buck–boost converter diodes. Furthermore, the DCM operation enables easy implementation of the control scheme. It can be noted that under constant duty cycle DCM operation, the input current is proportional to the input voltage at every switching cycle; therefore, the overall in-put current will be in-phase with microgenerator output voltage. The converter operation can be divided mainly into four modes. Mode-1 and Mode-2 are for the boost converter operation during the positive half cycle of the input voltage. Under Mode-1, the boost switch S_1 is ON and the current in the boost inductor builds. During Mode-2, the switch is turned OFF and the output capacitor is charged. The other two modes: Mode-3 and Mode-4 are for the buck–boost converter operation during the negative half cycle of the input voltage. Under Mode-3, the buck–boost switch S_2 is ON and current in the buck–boost inductor builds. During Mode-4, the buck–boost switch S_2 is turned OFF and the stored energy of the buck–boost inductor is discharged to the output capacitor. Detailed discussion of the various modes of operation of the converter is reported in [21].

A. Converter Analysis

Consider the input current waveform of the converter as shown in Fig. 5(a). It can be noted that during the boost converter operation, the input current i and the boost inductor current (i_{L1}) are equal, but during the buck–boost converter operation, the in-put current i and the current in buck–boost inductor (i_{L2}) are not equal. This is because, in the buck–boost converter the in-put current becomes zero during the switch turn OFF period (T_{OFF}). Therefore, in a switching cycle, the energy transferred to the output by a buck–boost converter is equal to the energy stored in the inductor, whereas, in the boost converter, the energy transferred to the output is more than the energy stored in

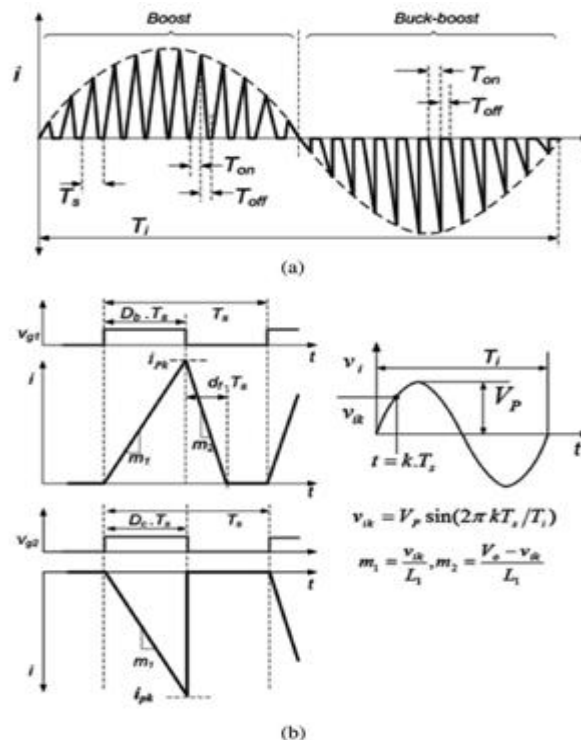


Fig. 5. (a) Input current waveform of the converter. (b) Input currents, gate drive signals and input voltage during a switching cycle of boost and buck–boost converter.

the inductor. Hence, for the equal duty cycles, input voltages and inductor values ($L_1 = L_2$), the total powers

delivered by the two converters over an input voltage cycle are not equal. In this section, analyses of the converters are carried out and the relations between the control and circuit parameters of the boost and the buck–boost converters pertaining to the input power and the output power are obtained.

Consider any k th switching cycle of the boost and the buck–boost converter as shown in Fig. 5(b), where T_s is the time period of the switching cycle, D_b is the duty cycle of the boost converter, $d_f T_s$ is the boost inductor current fall time (or the diode D_1 conduction time), D_c is the duty cycle of the buck–boost converter, v_i is the input voltage of the generator with amplitude V_p , and V_o is the converter output voltage. Assuming the switching time period (T_s) of the converter is much smaller than the time period of the input ac cycle (T_i), the peak value of the inductor current (i_{pk}) in the boost converter can be obtained as in (1)

$$i_{pk} = m_1 D_b T_s = \frac{v_{ik} D_b T_s}{L_1} \quad (1)$$

where $v_{ik} = V_p \sin\left(\frac{2\pi k T_s}{T_i}\right)$.

After the boost converter switch is turned OFF, the current in the inductor starts to fall (see Fig. 5). The slope (m_2) of this current is decided by the voltage across the inductor. In k th switching cycle, the voltage across the inductor during the inductor current fall time is: $V_o - v_{ik}$. Therefore, the inductor current fall time can be found as in (2)

$$d_f T_s = \frac{i_{pk}}{m_2} = \frac{i_{pk} L_1}{V_o - v_{ik}} \quad (2)$$

During this k th switching cycle, the total energy (E_{kb}) transferred from the input of the boost converter can be obtained as in (3)

$$E_{kb} = \frac{v_{ik} i_{pk} (D_b + d_f) T_s}{2} \quad (3)$$

The average power supplied in the boost switching cycle is

$$P_{kb} = \frac{E_k}{T_s} = \frac{v_{ik} i_{pk} (D_b + d_f)}{2} \quad (4)$$

The number of switching cycles during the time period of one input ac cycle is defined as $N = T_i / T_s$. In the proposed power electronics converter topology, the boost converter is operated for the half time period of the input ac cycle ($T_i / 2$). The average input power P_{ib} of the boost converter over this half cycle time period can be obtained as in (5)

$$P_{ib} = \left(\frac{2}{N}\right) \sum_{k=1}^{N/2} P_{kb} = \left(\frac{2}{N}\right) \sum_{k=1}^{N/2} \frac{v_{ik} i_{pk} (D_b + d_f)}{2} \quad (5)$$

For large N , the discrete function in (5) can be treated as a continuous function. The average input power of the boost converter P_{ib} (5) can be obtained by integrating the term in the summation over the half cycle ($T_i / 2$) period of the input ac voltage and then taking its mean value. The average power of the boost converter expressed in the integration form can be obtained as in (6)

$$P_{ib} = \frac{2}{T_i} \int_0^{T_i/2} \frac{D_b^2 T_s}{2L_1} V_p^2 \sin^2\left(\frac{2\pi}{T_i} t\right) \times V_o \left(V_o - V_p \sin\left(\frac{2\pi}{T_i} t\right)\right)^{-1} dt \quad (6)$$

where the microgenerator input voltage is defined as: $v_i = V_p \sin(2\pi t / T)$.

Simplifying (6), the average input power for the boost converter P_{ib} is found to be as follows:

$$P_{ib} = \frac{V_p^2 D_b^2 T_s}{4L_1} \beta$$

where

$$\beta = \left(\frac{2}{\pi}\right) \int_0^{\pi} \frac{1}{1 - (V_p/V_o) \sin \theta} d\theta$$

and

$$\theta = \frac{2\pi t}{T_i} \quad (7)$$

It can be noted that in (7), β is constant for fixed values of V_p and V_o . Also, it is seen that for large switching frequency of the converter, the average power is independent of the microgenerator output voltage frequency.

In steady state, the average input power of the converter is equal to the sum of the average output power and the various converter losses. Hence, by defining the converter efficiency as η for a load resistance R , the input power and the output power can be balanced as in (8)

$$\frac{V_p^2 D_b^2 T_s}{4L_1} \beta = \frac{V_o^2}{R} \frac{1}{\eta}. \quad (8)$$

From (8), the duty cycle of the boost converter (D_b) can be obtained as

$$D_b = \frac{2V_o}{V_p} \sqrt{\frac{L_1}{RT_s \eta}} \frac{1}{\beta}. \quad (9)$$

Further, consider the operation of the buck–boost converter; in this case the input power is supplied only during the ON period of the switch S_2 (see Fig. 3). During the OFF period of the switch S_2 , the input current is zero [see Fig. 5(a)]. Hence, for any k th switching cycle, the average power supplied by the buck–boost converter P_{kc} can be obtained as

$$P_{kc} = \frac{v_{ik} i_{Pk} D_c}{2}. \quad (10)$$

Applying similar approach, used earlier for the boost con-verter, the average power can be expressed in the integration form as

$$P_{ic} = \frac{2}{T_i} \int_0^{T_i/2} \frac{D_b^2 T_s}{2L_1} V_p^2 \sin^2 \left(\frac{2\pi}{T_i} t \right) dt = \frac{V_p^2 D_b^2 T_s}{4L_1}. \quad (11)$$

The duty cycle D_c can be obtained as in (12)

$$D_c = \frac{2V_o}{V_p} \sqrt{\frac{L_2}{RT_s \eta}}. \quad (12)$$

B. Converter Control Scheme

Using (9) and (12), the duty cycle of the boost converter D_b and the duty cycle of the buck–boost converter D_c can be related as

$$\frac{D_b}{D_c} = \sqrt{\frac{L_1}{L_2}} \frac{1}{\beta}. \quad (13)$$

Based on (13), two different control schemes can be proposed for the boost and buck–boost-based converter to deliver equal average input power. In scheme 1, the values of the inductors are kept to be equal ($L_2 = L_1$) and the converters are controlled with different duty cycles such that it satisfies the condition:

$$D_c = D_b \sqrt{\beta}.$$

In scheme 2, both the boost and the buck–boost converters are controlled with same duty cycle ($D_b = D_c$), whereas the inductor values are chosen to satisfy the condition: $L_1 = \beta L_2$. In Fig. 6, the variable β from (6) is plotted as a function of the step-up ratio (V_o/V_p). It can be seen from this plot that for large values of voltage step-up ratio, the value of β approaches to 1. Hence, for higher voltage step-up ratio applications, the boost and the buck–boost converters can be designed with inductors of equal values and they can be controlled with the same duty ratio to successfully deliver the required average power to the output.

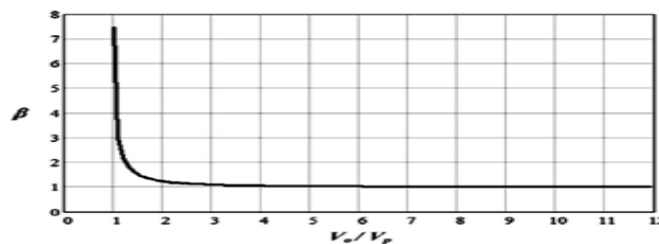


Fig. 6. β versus V_o/V_p (step-up ratio > 1) plot.

This is assistive for the target application of this study, where the very low voltage is stepped up to a

much higher dc out-put voltage. The proposed simplified control and design of the converter is later validated by simulation.

It can be mentioned that the value of β approaches to infinity for $V_o/V_p \rightarrow 1$. Therefore, from (7), the input power for the boost converter may seem to approach infinity as well. But in this case, the duty cycle of the boost converter D_b approaches to zero for $V_o/V_p \rightarrow 1$. Therefore, no power is transferred from the input to the output and the equation remains valid even when $V_o/V_p = 1$.

It can be mentioned that there could be two possible energy-harvesting scenarios. One, in which the converter is controlled to harvest maximum power available form the vibrating body and the microgenerator system and store it in an energy storage component (like battery) at the output. In this case, the output voltage is mainly decided by characteristics of the energy storage component. In the second scenario, the converter is controlled to harvest the amount of power demanded by the load while maintaining the desired output voltage. In this paper, the second scenario is considered to control the converter.

II. DESIGN GUIDELINE

The key design steps for this converter are to select the MOS-FETs, inductors, and the switching frequency of the converter. For a given microgenerator and a load, the input and output voltages are specified. Therefore, in this case, the voltage rating of the MOSFETs are decided by the output voltage of the converter. The current rating of the MOSFETs has to be decided by the designer. It can be noted that the MOSFET carries maximum current at the peak of the input voltage [see Fig. 5(a)]. The maximum current I_{max} of the converter can be obtained as in (14)

$$I_{max} = \frac{V_p D}{L f_s} \quad (14)$$

Where f_s is the switching frequency of the converter, L is the inductance value for both boost and buck–boost converters, and D is the duty cycle of the converters ($D = D_b = D_c$).

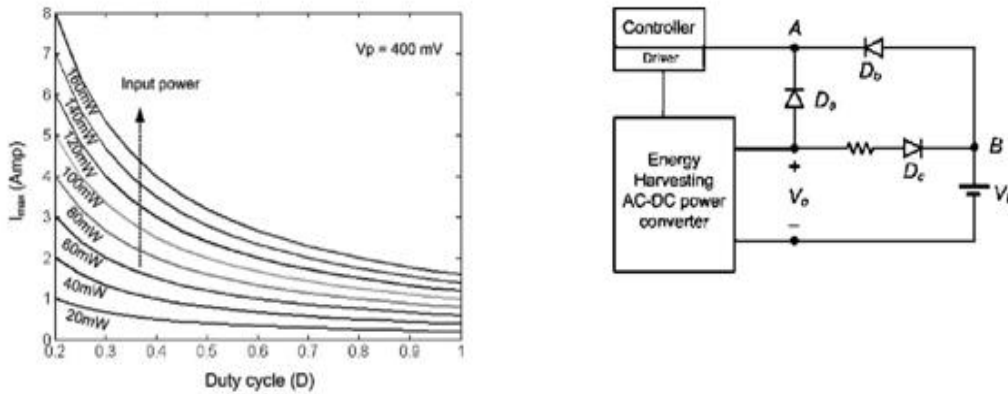


Fig. 8. Proposed auxiliary self-starting circuit using a battery.

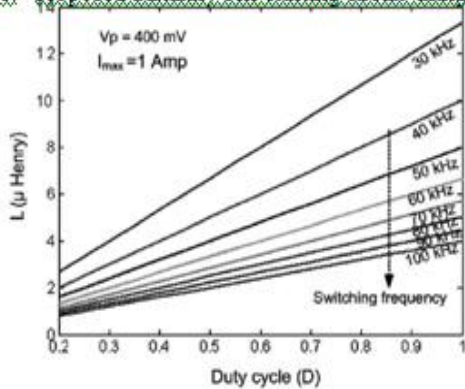


Fig. 7. Design graphs. (a) Duty ratio versus maximum input current. (b) Duty ratio versus inductance.

Power. The duty cycle and the frequency of the converter can be appropriately selected to choose the desired value of the inductor. In this study, the proposed converter is designed to supply about 55 mW of power to the load.

IV. SELF-STARTING CIRCUIT AND CONTROL CIRCUIT

In a practical energy-harvesting scenario, the controller and the MOSFET driver circuit of the converter are required to be self-starting and they should be powered by the energy harvesting system. In this study, an auxiliary self-starting circuit, as shown in Fig. 8, is proposed to power the controller and the drivers at the beginning, when the converter starts up. The proposed self-starting auxiliary circuit utilizes a battery and Schottky diodes for this purpose (see Fig. 8). For the successful operation of this self-starting circuit, the battery nominal voltage V_b should be less than the target output voltage V_o minus the forward voltage drop of a diode V_f , and it should be above the minimum voltage requirements of the controller and driver circuits

From (11) and (14), the maximum current can be expressed as a function of average input power P_{in} as in (15)

$$I_{max} = \frac{4P_i}{V_p D} \quad (15)$$

$V_p D$

In Fig. 7(a), the relationship between the maximum input current and the duty cycle for different input power is shown.

Using this chart, the MOSFET current rating and converter duty cycle can be selected. With these selected values the MOSFET maximum current, the inductor value and the switching frequency can be obtained from (14). The relationship between the value of the inductor (L) and the duty cycle over a range of switching frequency is shown in Fig. 7(b).

Using these charts and the equations, the initial values of the key components of the converter can be decided. Further, optimum values of the components can be selected by carrying out detailed loss analysis of the converter and minimizing the losses. It can be noted that the value of the maximum current (I_{max}) changes proportionally with the input power (P_{in}) of the converter. Therefore, the size of the MOSFET can be scaled as per the power requirement of the load. This is applicable for even low-power applications, demanding less than 1 mW of

In this study, the target output voltage $V_o = 3.3$ V and forward voltage drop of the diodes $V_f = 0.22$ V. A battery with nominal voltage $V_b = 3$ V is selected for the self-starting. At the beginning of the converter operation, when the output voltage V_o is not available, the controller and the driver circuit will be powered by the battery through the Schottky diode D_b . This will allow the converter to charge the output capacitor to the reference voltage. In steady state, when the output voltage has reached the value 3.3 V, the diode D_b would be reverse biased, therefore, the battery will not be powering the controller and the driver. At this time, they will be powered from the converter output through the diode D_a . During this condition, the battery will remain under floating condition. It can be noted that only a very small amount of energy is taken from the battery for the startup of the energy harvesting system. Furthermore, the used energy of the battery can be replenished by recharging it from the output of converter through the diode D_c . Therefore, the entire amount of energy used for the converter operation, including the energy used during its starting, is harvested from the ambience. Therefore, with proper design and selection of

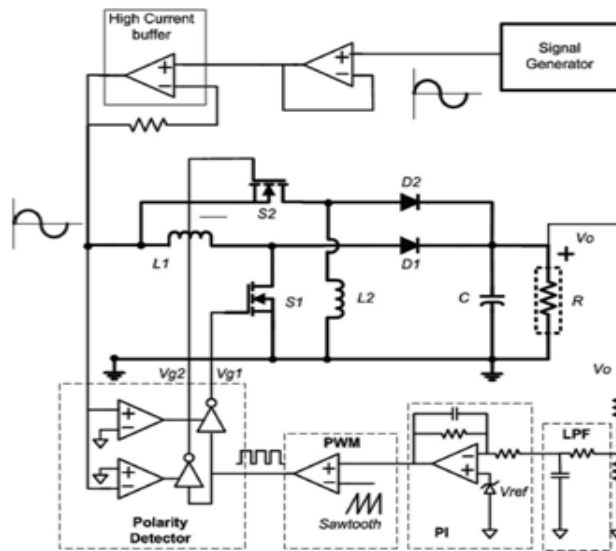


Fig. 9. Circuit diagram of the energy-harvesting converter.

the components, this auxiliary circuit can be used to operate the energy harvesting system virtually for indefinite period of time.

The circuit diagram for the implementation of the proposed energy-harvesting converter and its control scheme is presented in Fig. 9. The sensed output voltage of the converter is processed by a low-pass filter. The processed signal is compared with the reference voltage V_{ref} . The error signal is used by the PI controller to estimate the control voltage that is compared with a saw-tooth waveform in the pulse width modulator (PWM). The pulse signal produced by the PWM is fed to the two buffers that can be enabled by external signals. The comparators in the polarity detector unit enable the appropriate buffers to produce the gate pulses (V_{g1} and V_{g2}) that control the MOSFETs of the boost and buck–boost converter during appropriate half cycles.

In this study, the resonance-based electromagnetic microgenerator is modeled as an ac voltage source. A signal generator followed by a high-current buffer is used to realize the micro-generator output voltage (see Fig. 9). This buffer can be realized by using a power operational amplifier in voltage follower mode. Further, it can be mentioned that the self-resistance and self-inductance of the electromagnetic microgenerator are very small, therefore, the self-impedance of the microgenerators are not included for the analysis of the proposed converter operation. However, it can be incorporated in the analysis, for the prediction of the performances of the entire energy harvesting system.

V. SIMULATION RESULTS

A resonance-based electromagnetic microgenerator, producing 400 mV peak sinusoidal output voltage, with 100-Hz frequency is considered in this study for verification of the proposed converter topology (see Fig. 3). The closed-loop simulation

TABLE I
CIRCUIT COMPONENTS OF THE CONVERTER

Circuit Components	Name	Ratings
Inductor	L_1, L_2	4.7 μ H
Inductor resistance	R_l	30 m Ω
N - channel MOSFET	S_1, S_2	20V, 2A
MOSFET on state resistance	$R_{ds, on}$	150 m Ω @ $V_{gs}=3V$
Schottky Diode	D_1 & D_2	23V, 1A
Schottky Diode forward voltage	V_f	0.23V
Load resistance	R	200 Ω
Capacitor	C	68 μ F
Capacitor ESR	R_c	30 m Ω

tion of the converter is carried out based on the control schemes presented in Section II. The reference output voltage (V_{ref}) is considered to be 3.3 V. The energy-harvesting converter is designed for supplying power to a 200- Ω load resistance, hence, supplying about 55 mW of output power.

The converter design is carried out based on the analysis and design guidelines, discussed earlier in the

Sections II and III. Commercially available MOSFET (Si3900DV from *Vishay*) is selected to realize the switches S_1 and S_2 . The forward volt-age of the selected MOSFET body diode is about 0.8 V, which is higher than the peak of the input voltage. This inhibits any reverse conduction in the MOSFETs. The nominal duty cycle of the converter is chosen to be 0.7. The inductor is designed to have a standard value of $4.7 \mu\text{H}$ and commercially available inductor (IHLP-2525CZ from *Vishay*) is used to realize L_1 and L_2 . Based on these designed values, the switching frequency of the converter is selected to be 50 kHz [see Fig. 7(b)]. The diodes, D_1 and D_2 are chosen to be schottky type with low forward voltage (0.23 V, NSR0320 from *ON Semiconductor*). The output capacitor value is $68 \mu\text{F}$. The converter simulations are carried out in *Saber*. Circuit models of the selected devices and components, available from the manufacturers, are used in the simulations. Various values for circuit components of the designed converter are presented in Table I. To verify the proposed control techniques, at first simulation is carried out for the control scheme1, using $L_2 = L_1 = 4.7 \mu\text{H}$ and the duty ratio of the two converters are not equal. In the simulation, the duty cycle of the boost converter D_b is estimated by a PI controller (see Fig. 3). The buck–boost converter duty cycle D_c is calculated from the estimated duty cycle D_b and (13). The input current of the boost converter (see i_b in Fig. 3) and the input current of the buck–boost converter (see i_c in Fig. 3) for load resistance $R = 200 \Omega$ is shown in Fig. 10(a) and (b), respectively. The total input current and the microgenerator output voltage (v_i) are shown in Fig. 10(c). It can be seen that the boost converter

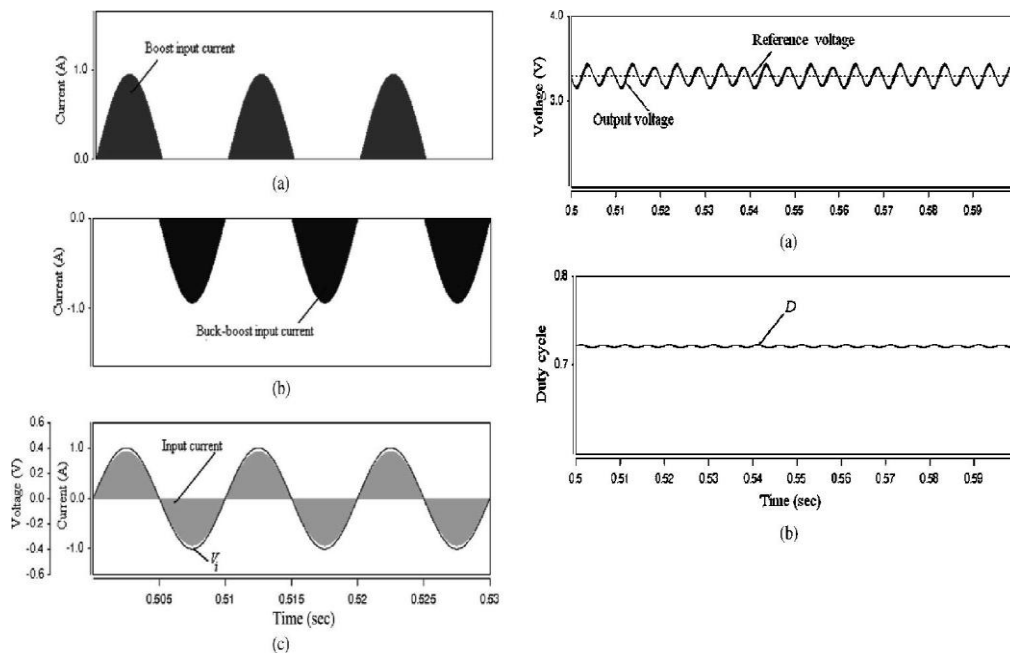


Fig. 10. (a) Boost input current, (b) buck–boost input current, and (c) total input current with ac input voltage for $R = 200 \Omega$ and $L_1 = L_2$.

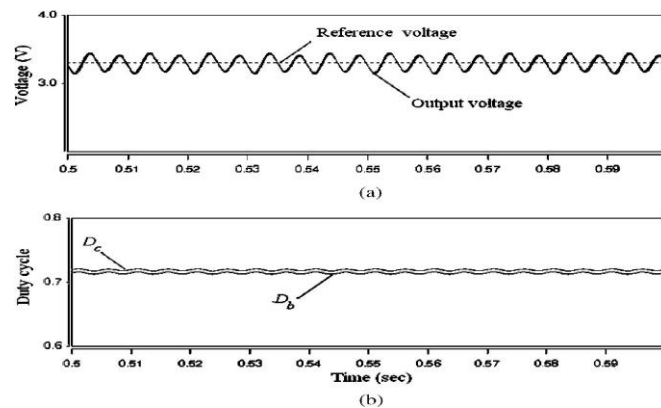


Fig. 11. (a) Output voltage and (b) duty cycle values of the boost converter (D_b) and buck–boost converter (D_c) for $R = 200 \Omega$ and $L_1 = L_2$.

is operated during the positive half cycle, while the buck–boost converter is operated during negative half cycle of the microgen-erator output voltage. The converter output voltage and the duty cycles, estimated by the controller are shown in Fig. 11(a) and (b), respectively. The output voltage ripple is about ± 0.14 V, which is

$\pm 4.24\%$ of the nominal output voltage. The estimated efficiency of the converter is 63%. For this operating condition, the duty cycle calculated from the analysis of Section II is $D_b = 0.71$. It can be noted from Fig. 11(b) that the estimated duty

Fig. 12. (a) Output voltage and (b) duty cycle of the converters ($D = D_b = D_c$), for $R = 200 \Omega$ and $L_1 = L_2$. cycle by the controller in the circuit simulation closely matches with value of the duty cycle calculated analytically.

In this study, the output voltage to input voltage peak step-up ratio is: $V_o/V_p = 8.25$. Furthermore, from Fig. 11(b) it is found that the operating duty ratios of the boost and the buck–boost converters are almost same. These corroborate the earlier conclusion from the analysis in Section II (see Fig. 6) that for high step-up ratio, the duty cycles of the converters with same inductor values will be almost equal. Hence, to achieve simple control structure, less component counts and for all other practical advantages, both the boost converter and the buck–boost converter can be controlled with same duty cycle for such high step-up applications. To validate this proposed control scheme, further simulations of the converter is carried out for load resistance $R = 200 \Omega$ when the boost and buck–boost converter are controlled with same duty ratio. Fig. 12(a) and (b) present the output voltage and the duty cycle of the converter, respectively. It can be seen from these figures that with the equal duty ratio control, the converter can successfully produce the desired output voltage with similar voltage ripple.

To verify the operation of the converter under different load conditions, the load resistance is increased to $R = 400 \Omega$. The input voltage, input current, and the estimated duty cycle by the controller are shown in Fig. 13(a). For this load condition, the duty cycle value is about $D = 0.49$. This matches with calculated duty cycle from previous analysis of Section III ($D = 0.5$). The output voltage under this load condition is shown in Fig. 13(b).

The simulations are carried out with the self-starting circuit (see Fig. 8) proposed for the converter in Section IV. The battery of the self-starting circuit is modeled as a constant voltage source of 3.0 V. During start-up period of the converter, the power consumed by the control circuit from the battery and the converter is presented in Fig. 14. The battery voltage level and the output voltage of the converter are also shown in this

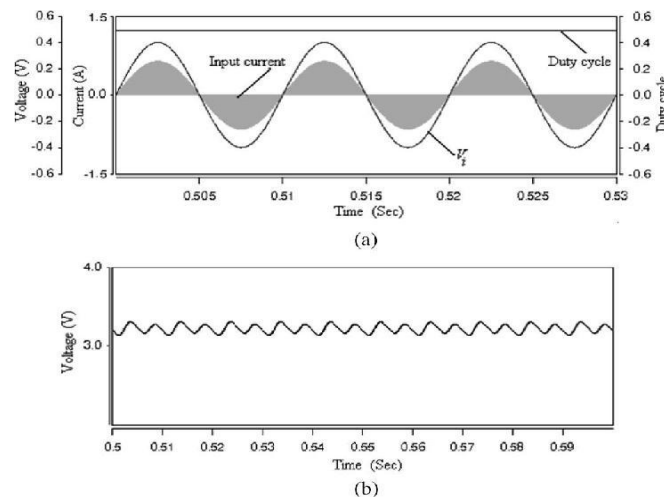


Fig. 13. (a) Input current, ac input voltage, and duty cycle ($D = D_b = D_c$) and (b) output voltage for $R = 400 \Omega$ and $L_1 = L_2$.

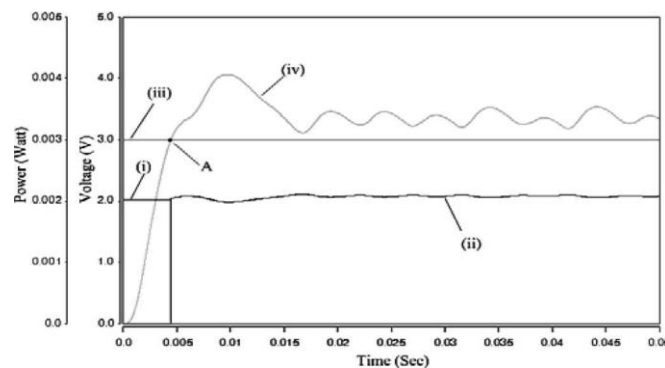


Fig. 14. Power and voltages during self start-up. Curves (i), (ii), (iii), and (iv) show the power supplied by the battery, power draw from the converter output, battery voltage, and converter output voltage, respectively.

figure. It can be seen from these plots that at the beginning, when the converter output voltage is building, the power consumed by the control circuit is only supplied by the battery. At point A, as shown in Fig. 14, the converter output voltage becomes higher than the battery voltage. From this point onwards, the power consumed by the control circuit is supplied by the converter, and the power draw from the battery becomes zero (see Fig. 14). It can be found that the start-up time taken by the converter is about 4.6 ms. This is less than the half cycle period of the input ac voltage (100 Hz). Further, it can be obtained that the average power consumed by the control circuit is about 2.2 mW.

VII. CONCLUSION

The presented direct ac-to-dc low voltage energy-harvesting converter avoids the conventional bridge rectification and achieves higher efficiency. The proposed converter consists of a boost converter in parallel with a buck–boost converter. The negative gain of the buck–boost converter is utilized to boost the voltage of the negative half cycle of the microgenerator to positive dc voltage. Detailed analysis of the converter for direct ac-to-dc power conversion is carried out and the relations between various converter circuit parameters and control parameters are obtained. Based on the analysis, a simplified control scheme is proposed for high-voltage step-up application. Design guide-lines are presented for selecting values of the key components and control parameters of the converter. A self-startup circuit, using a battery only during the beginning of the converter operation, is proposed for the energy-harvesting converter. Operation and the implementation of the self-startup circuit and the control circuit of the converter are presented in details. Based on the analysis and the design guidelines, a prototype of the converter is developed. The proposed control scheme with the self-startup circuit is implemented and the converter is successfully operated to directly step-up the low ac voltage to a high dc voltage. The loss components of the converter are estimated. The measured efficiency of the converter is 61%, which is higher than the reported converters.

REFERENCES

- [1] J. A. Paradiso and T. Starner, “Energy scavenging for mobile and wireless electronics,” *IEEE Pervasive Comput.*, vol. 4, no. 1, pp. 18–27, Jan./Mar. 2005.
- [2] S. Meninger, J. O. Mur-Miranda, R. Amirtharajah, A. P. Chandrakasan, and J. H. Lang, “Vibration-to-electric energy conversion,” *IEEE Trans. Very Large Scale Integr. Syst.*, vol. 9, no. 1, pp. 64–76, Feb. 2001.
- [3] M. El-Hami, P. Glynne-Jones, N. M. White, M. Hill, S. Beeby, E. James, D. Brown, and J. N. Ross, “Design and fabrication of a new vibration-based electromechanical power generator,” *Sens. Actuators A: Phys.*, vol. 92, pp. 335–342, 2001.
- [4] T. M. Thul, S. Dwari, R. D. Lorenz, and L. Parsa, “Energy harvesting and efficient power generation from human activities,” in *Proc. Center Power Electron. Syst. (CPES) Semin.*, Apr. 2007, pp. 452–456.
- [5] N. G. Stephen, “On energy harvesting from ambient vibration,” *J. Sound Vibrations*, vol. 293, pp. 409–425, 2006.
- [6] J. R. Amirtharajah and A. P. Chandrakasan, “Self-powered signal processing using vibration-based power generation,” *IEEE J. Solid-State Circuits*, vol. 33, no. 5, pp. 687–695, May 1998.
- [7] B. H. Stark, P. D. Mitcheson, M. Peng, T. C. Green, E. Yeatman, and
- [8] S. Holmes, “Converter circuit design, semiconductor device selection and analysis of parasitics for micropower electrostatic generators,” *IEEE Trans. Power Electron.*, vol. 21, no. 1, pp. 27–37, Jan. 2006.
- [9] C. B. Williams and R. B. Yates, “Analysis of a micro-electric generator for microsystems,” in *Proc. Int. Conf. Solid-State Sens. Actuators*, 1995, pp. 369–372.
- [10] P. D. Mitcheson, T. C. Green, E. M. Yeatman, and A. S. Holmes, “Architectures for vibration-driven micropower generators,” *J. Microelectromech. Syst.*, vol. 13, no. 3, pp. 429–440, Jun. 2004.
- [11] S. Xu, K. D. T. Ngo, T. Nishida, G. B. Chung, and A. Sharma, “Low frequency pulsed resonant converter for energy harvesting,” *IEEE Trans. Power Electron.*, vol. 22, no. 1, pp. 63–68, Jan. 2007.
- [12] J. Elmes, V. Gaydarzhiev, A. Mensah, K. Rustom, J. Shen, and I. Batarseh, “Maximum energy harvesting control for oscillating energy harvesting systems,” in *Proc. IEEE Power Electron. Spec. Conf.*, Jun. 2007, pp. 2792–2798.
- [13] S. P. Beeby, R. N. Torah, M. J. Tudor, P. Glynne-Jones, T. O’Donnell, R. Saha, and S. Roy, “Micro electromagnetic generator for vibration energy harvesting,” *J. Micromech. Microeng.*, vol. 17, pp. 1257–1265, 2007.
- [14] B. H. Stark, P. D. Mitcheson, M. Peng, T. C. Green, E. Yeatman, and S. Holmes, “Converter circuit design, semiconductor device selection and analysis of parasitics for micropower electrostatic generators,” *IEEE Trans. Power Electron.*, vol. 21, no. 1, pp. 27–37, Jan. 2006.
- [15] T. Paing, J. Shin, R. Zane, and Z. Popovic, “Resistor emulation approach to low-power RF energy

- harvesting,” *IEEE Trans. Power Electron.*, vol. 23, no. 3, pp. 1494–1501, May 2008.
- [16] E. Lefeuvre, D. Audigier, C. Richard, and D. Guyomar, “Buck-boost converter for sensorless power optimization of piezoelectric energy harvester,” *IEEE Trans. Power Electron.*, vol. 22, no. 5, pp. 2018–2025, Sep. 2007.
- [17] X. Cao, W.-J. Chiang, Y.-C. King, and Y.-K. Lee, “Electromagnetic energy harvesting circuit with feedforward and feedback DC–DC PWM boost converter for vibration power generator system,” *IEEE Trans. Power Electron.*, vol. 22, no. 2, pp. 679–685, Mar. 2007.
- [18] G. K. Ottman, H. F. Hofmann, and G. A. Lesieutre, “Optimized piezoelectric energy harvesting circuit using step-down converter in discontinuous conduction mode,” *IEEE Trans. Power Electron.*, vol. 18, no. 2, pp. 696–703, Mar. 2003.
- [19] G. K. Ottman, H. F. Hofmann, A. C. Bhatt, and G. A. Lesieutre, “Adaptive piezoelectric energy harvesting circuit for wireless remote power supply,” *IEEE Trans. Power Electron.*, vol. 17, no. 5, pp. 669–676, Sep. 2002.
- [20] M. Ferrari, V. Ferrari, D. Marioli, and A. Taroni, “Modeling, fabrication and performance measurements of a piezoelectric energy converter for power harvesting in autonomous microsystems,” *IEEE Trans. Instrum. Meas.*, vol. 55, no. 6, pp. 2096–2101, Dec. 2006.
- [21] P. D. Mitcheson, T. C. Green, E. M. Yeatman, and A. S. Holmes, “Power processing circuits for electromagnetic, electrostatic and piezoelectric inertial energy scavengers,” *Microsyst. Technol.*, vol. 13, pp. 1629–1635, May 2007.
- [22] S. Dwari, R. Dayal, and L. Parsa, “A novel direct AC/DC converter for efficient low voltage energy harvesting,” in *Proc. IEEE Ind. Electron. Soc. Annu. Conf.*, Nov. 2008, pp. 484–488. Richelli, L. Colalongo, S. Tonoli, and Z. M. Kovács-Vajna, “A 0.2–1.2 V DC/DC boost converter for power harvesting applications,” *IEEE Trans. Power Electron.*, vol. 24, no. 6, pp. 1541–1546, Jun. 2009.
- [23] J. C. Salmon, “Circuit topologies for single-phase voltage-doubler boost rectifiers,” *IEEE Trans. Power Electron.*, vol. 8, no. 4, pp. 521–529, Oct. 1993.